Russian Journal of Earth Sciences

Modeling the Horizontal Velocity Field of the Earth's Crust in a Regular Grid from GNSS Measurements

Alexander I. Manevich[*,1,2], **Iliya V. Losev**[1], **Alina M. Avdonina**[1], **Roman V. Shevchuk**[1,3], **Vladimir I. Kaftan**[1], **and Viktor N. Tatarinov**[1,3]

[1] Geophysical Center RAS, Moscow, Russia
[2] National University of Science and Technology MISIS, College of Mining, Moscow, Russia
[3] Schmidt Institute of the Physics of the Earth RAS, Moscow, Russia
* **Correspondence to:** Alexander I. Manevich, a.manevich@gcras.ru.

Abstract: There are numerous methods for modeling velocity fields of the Earth's crust. However, only a few of them are capable of modeling data beyond the contour of the geodetic network (extrapolating). Spatial modeling based on a neural network approach allows for the adequate modeling of the field of recent crustal movements and deformations of the Earth's crust beyond the geodetic network contour. The study extensively examines the hyperparameter settings and justifies the applicability of the neural network model for predicting crustal movement fields using the Ossetian geodynamic polygon as an example. The presented results, when compared to classical modeling methods, demonstrate that the neural network approach confidently yields results no worse than classical methods. The results of modeling for the Ossetian polygon can be used for geodynamic zoning, identification zones of extension and compression, computing the tectonic component of stresses, and identifying areas of high-gradient displacements.

Keywords: velocity fields, resent crustal movements, spatial modeling, regular grid, extrapolation, interpolation, artificial neural networks.

Citation: Manevich, A. I., I. V. Losev, A. M. Avdonina, R. V. Shevchuk, V. I. Kaftan, and V. N. Tatarinov (2023), Modeling the Horizontal Velocity Field of the Earth's Crust in a Regular Grid from GNSS Measurements, *Russian Journal of Earth Sciences*, 23, ES6002, EDN: IXIPOZ, https://doi.org/10.2205/2023es000885

1. Introduction

Recent crustal movements (RCM), especially in seismically active areas within zones of active tectonic faults, can lead to natural disasters and accidents at hazardous industrial facilities. These facilities include linear main gas and oil pipelines, hydraulic structures, radiation hazardous sites, chemical plants, etc. [*Batugin et al.*, 2022; *Tatarinov et al.*, 2019]. Each year, new technologies and protective measures are developed. They are aimed at reducing the number of accidents and the associated social, economic, and environmental consequences. The exploration of new territories, the complexification of mineral extraction conditions, and industrial technological processes result in stricter industrial safety requirements. According to regulatory requirements, deformation monitoring of the geological environment is an integral and crucial part of the system ensuring the safety of engineering structures. Deformation monitoring involves periodic geodetic observations, accompanied by analysis, interpretation of observation results, and an ensuing evaluation of the geological environment's condition.

The most common measurement tools for monitoring RCM are Global Navigation Satellite Systems (GNSS). GNSS tools are used to measure displacements of points at geodynamic sites in the vicinity of engineering objects. However, due to various circumstances, ensuring the sufficiency and reliability of the initial data is not always possible. The insufficiency of data for studying RCM parameters is caused by the following reasons [*Bogusz et al.*, 2013; *Manevich et al.*, 2022; *Shen et al.*, 1996, 2015]:

- limited availability of dense networks and a sufficient number of points for continuous instrumental observations operating over a long period.

Research Article

Received: 30 November 2023
Accepted: 24 December 2023
Published: 30 December 2023

- complex organization of measurements in both field campaigns and continuous observations.
- inability to establish a proper structure for geodynamic sites due to economic, physical-geographical, and social conditions.
- difficulty in accessing instrumental measurement data at geodynamic sites (both governmental and academic).
- a low number of highly accurate continuously operating GNSS stations with open access to measurement data.

Figure 1 presents an example of the Ossetian geodynamic polygon [*Mironov et al.*, 2021]. It is evident that the GNSS network contour is disproportionately elongated in the southwest-northeast direction. Due to complex physical geographical conditions, approximately 3/4 of the entire territory lies outside the measurement network's contour. Consequently, obtaining surface movement values for this area is unattainable. This affects the assessment of internal deformations. This happens because the triangles along the edges are comparable in area to the entire polygon's contour, while those along the diagonal are too distant from an equilateral Figure 1. The configuration of the finite elements is not optimal for deformation analysis. This deteriorates the accuracy of deformation component calculations and complicates their geometric interpretation [*Dokukin et al.*, 2010; *Wu et al.*, 2003].

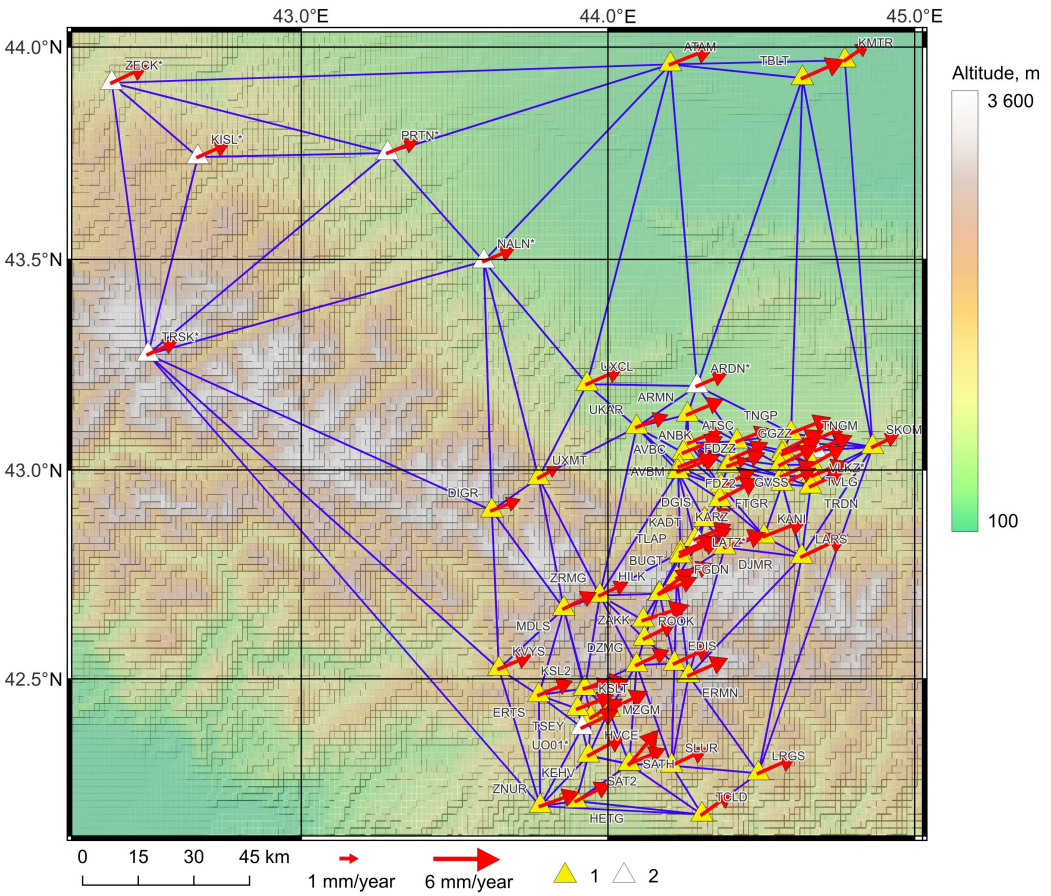

Figure 1. Geodynamic polygon of the Ossetia [*Mironov et al.*, 2021]. 1 – periodically measured geodetic points; 2 – continuously operating geodetic points.

In geodynamics, the parameters of planned surface deformations are determined at specific points, assuming that sections of the Earth's crust are uniformly deformed. Typically, the geodetic network is divided into triangles, and the obtained deformation tensor components are associated with their geometric centers. There is an approach in deformation field calculations that does not involve triangular finite elements. This

approach utilizes points falling within a defined survey radius, assigning them weighting coefficients based on their distance from the deformation reference point. One of the most prevalent methods for computing the deformation tensor field is outlined in the study by [*Shen et al.*, 1996], and it is implemented in the software packages grid_strain and grid_strain3 [*Teza et al.*, 2008]. The assessment of observation point weights is performed according to a prescribed analytical function [*Shen et al.*, 1996, 2015]. The weight of the displacement values is inversely proportional to the mathematical expectation of the measure of crustal deformation heterogeneity between the interpolated point and the observation point. However, using such a weighting function can pose a problem in incorrectly assessing observation point weights as these functions fail to account for the crustal heterogeneities. Unjustified weight assignments can lead to significant distortions in the results. Thus, it is crucial to have robust justifications when selecting a specific weighting function.

The primary uncertainty in deformation field calculations stems from the lack of a physical understanding of the deformed geological environment. This leads to subsequent uncertainties in interpreting its deformation. Distance weighting methods create complex geometric shapes with difficult interpretation. The triangular network method of calculation strictly associates a physically defined area within the finite element on the geodetic network, enabling a clear interpretation of its deformation derived from precise displacement values at its vertices. Another perspective method is to interpolate the data onto a regular grid to obtain uniformly distributed data throughout the entire study area.

The interpolation model allows obtaining regular data at grid nodes across the entire study area. Therefore, in deformation monitoring based on GNSS measurements, there is a pressing issue of analyzing data when there is an insufficient quantity available. Moreover, computations based on irregular geodetic network data may lead to a significant loss of accuracy in determining displacements and deformation components. This is consequently increasing the unreliability of the derived estimations and predictions [*Dokukin et al.*, 2010; *Wu et al.*, 2003]. To obtain regular (grid) data on surface deformations, it is necessary to employ methods of mathematical modeling of displacement fields. For instance, in [*Aleshin et al.*, 2022; *Allmendinger et al.*, 2011; *Esikov*, 1979], it is noted that due to the complexity of calculating deformation parameters, it is advisable to choose regions where more complex deformed conditions should be specified within the finite element (where deformation is typically assumed to be uniformly distributed), thereby enhancing the order of approximation of the data. There are numerous methods for modeling field movements (which will be discussed below). However, only some of them can model data beyond the geodetic network contour (extrapolate data). Artificial neural networks constitute one such family of methods, showing extensive promise in this area of research. Therefore, the goal of this study is to study the potential for modeling the field of recent horizontal crustal movements on a regular data grid. This is done based on GNSS measurements using a neural network approach and substantiating the parameters of the neural network algorithm for this specific task.

2. Materials and Methods

2.1. Interpolation models

The main methods for modeling recent Earth's surface movements are discussed below. These methods can be divided into two major groups:

- deterministic methods: These methods involve the physical description of a specific model for the movements of a geological process or phenomenon. These models are commonly used for modeling displacement fields during earthquakes [*Lei and Loew*, 2021; *Okada*, 1992], fault slip displacements [*Aki*, 1968; *IAEA-TECDOC-1987*, 2021; *Moss and Ross*, 2011; *Nurminen et al.*, 2020; *Youngs et al.*, 2003], surface subsidence due to mining operations [*Kuzmin*, 2020; *Mazurov*, 2016; *Petrov et al.*, 2021], and so on.
- interpolation and extrapolation methods: These methods do not rely on physical representations of the environment. They are universal for generating gridded data

for movement and deformation fields regardless of the studied geological process or phenomenon. These methods include geostatistical methods [*Bogusz et al.*, 2013; *Ghiasi and Nafisi*, 2015], distance-weighting methods [*Bogusz et al.*, 2013; *Shen et al.*, 1996, 2015], spline and polynomial methods [*Bogusz et al.*, 2013; *Sandwell*, 1987], machine learning methods [*Aleshin et al.*, 2022; *Grishchenkova*, 2017; *Manevich et al.*, 2021; *Manevich and Tatarinov*, 2017; *Tatarinov et al.*, 2018], and others.

Spline functions are the most frequently used methods, serving as a reliable and effective tool for approximating and interpolating various geophysical data, including surface movements [*Bogusz et al.*, 2013; *Markovich*, 2020; *Sandwell*, 1987]. Several types of spline functions are known to be applied in the field of surface movement interpolation. Primarily, cubic spline functions are utilized to create smooth surfaces from a set of unevenly distributed points in space. The physical interpretation of the cubic spline corresponds to the application of force to an elastic material (like a rod or layer), approximating it to a model of elastic crustal deformation. The spline interpolation method minimizes the surface's curvature function, which passes through all original points within the accuracy of their average errors. At the original data points, the curvature of the function is at a minimum, while between the points, the function's surface is close to linear. All original data points contribute to the modeled value [*Bogusz et al.*, 2013].

Another method commonly used in practice is the Shen method [*Shen et al.*, 1996]. This approach employs GNSS stations within a specified survey radius, assigning them weighting coefficients based on their distance from the reference point of deformation. The technique has been implemented in several software packages for deformation analysis, such as grid_strain and grid_strain3 [*Teza et al.*, 2008], SSPX [*Cardozo and Allmendinger*, 2009], Geostrain [*Goudarzi et al.*, 2015], PyStrain [*Dimitrios et al.*, 2019], among others. The assessment of observation point weights is performed according to a prescribed analytical function [*Shen et al.*, 1996]. The weight of the displacement value is inversely proportional to the mathematical expectation of the degree of crustal deformation heterogeneity between the interpolated point and the observation station. In essence, the approach emphasizes that the closer the GNSS station is to the studied point, the more significant its contribution.

In modeling recent crustal movement fields, classical spatial interpolation methods are regularly employed, such as the inverse distance method, kriging, and the natural neighbour method [*Bogusz et al.*, 2013; *Ghiasi and Nafisi*, 2015; *Matheron*, 1970; *Shen et al.*, 2015; *Srivastava and Isaaks*, 1989; *Wackernagel*, 1994]. Their application is justified by their ease of implementation in GIS environments and the ability to finely tune parameters. However, it is essential to select the search radius correctly when using these methods. If the search radius is set too large, the modeled data will be excessively smoothed and averaged. Conversely, if the radius is set too small, the nearest neighbour effect may be observed, where the modeled value is increasingly similar to the nearest known point. It is important to note that the Shen method, to some extent, resembles the inverse distance method but employs a different weighting function.

The next method is based on formulating multiple regression equations, where the regressors are not statistically derived coefficients but a set of geological-geophysical parameters of the studied area. It is worth noting that in modern GIS packages, this approach is referred to as geographic weighted regression, essentially denoting the same process. One of the initial mentions of using this approach for predicting recent crustal movements can be traced back to the work of [*Kolmogorova and Karataev*, 1975]. However, its application is also seen in recent crustal movement research [*Markovich*, 2020]. This method works well for building regional models of recent crustal movements over large territories. The large scale allows the utilization of a more extensive array of geological-geophysical parameters, the variability of which is less significant for local areas.

The focus should also be on machine learning methods. The most prominent among them is the artificial neural network (ANN) method. Experience in its application is known for predicting ground subsidence caused by mining activities [*Boubou et al.*, 2010; *Grishchenkova*, 2017], modeling post-seismic deformations [*Yamaga and Mitsui*, 2019],

forecasting landslide movements [*Yang et al.*, 2019], volcanic deformations [*Anantrasirichai et al.*, 2018], and slow tectonic movements fields [*Manevich et al.*, 2021; *Manevich and Tatarinov*, 2017; *Tatarinov et al.*, 2018].

The algorithm represents a layered system of interconnected and interacting simple processors (neurons). Each network neuron deals only with the signals it receives and those it sends to other neurons. When connected in a sufficiently large network, these individually simple neurons together are capable of performing rather complex tasks. The network involves interconnections between neurons, and the strength of these connections is expressed by specific weighting coefficients. The complete matrix of these weighting coefficients, along with the input and output signals of the neurons essentially constitutes the decision-making apparatus of this method. Neurons interacting with each other are organized in layers (involving input, hidden, and output layers). The task of neurons in the input layer is to receive, normalize, and transmit information to the hidden layers. Further calculations of signals transmitted to subsequent hidden layers or the output layer take place in the hidden layers of the artificial neural network. The output layer transforms the final signals into output information for the user of the artificial neural network.

To train an artificial neural network (essentially tuning the synaptic weight coefficients), datasets are formed with known predictable data. Then the network is iteratively trained by comparing its predicted value with the actual value until they match within a certain (user-defined) margin of error. Once the training is completed, the network can use its weight coefficient matrix for prediction. Let's take a closer look at the training process of the artificial neural network. There is a set of data entering the input layer of the network:

$$\sum y_n = \begin{pmatrix} y_1 \\ y_2 \\ \cdots \\ y_n \end{pmatrix} \rightarrow \overline{y_n} = \begin{pmatrix} \overline{y_1} \\ \overline{y_2} \\ \cdots \\ \overline{y_n} \end{pmatrix},$$

where $y_1, y_2, \ldots, y_n$ – input data; $\overline{y_1}, \overline{y_2}, \ldots, \overline{y_n}$ – normalized input data, for distribution into ANN layers.

To work with the incoming data within the network, it's necessary to process them by normalizing them, which means representing numerical parameters not in absolute units, but in some dimensionless units characterizing their relative values. Then the signals are passed to the hidden layer, being multiplied by the respective weight coefficients (initially set randomly).

$$S_n = \overline{y_n} \times W_{ij} = \begin{pmatrix} \overline{y_1} \\ \overline{y_2} \\ \cdots \\ \overline{y_n} \end{pmatrix} \times \begin{pmatrix} w_{11} & \cdots & w_{i1} \\ \cdots & \cdots & \cdots \\ w_{1j} & \cdots & w_{ij} \end{pmatrix},$$

where W_{ij} – full matrix of synapse weighting coefficients; $w_{11}, w_{12}, \ldots, w_{ij}$, – weighting coefficients of synapses; i – number of the hidden layer; j – synapse number in the layer.

In each neuron of the hidden layer, the incoming signals are summed, followed by the activation (through a specially chosen function) of a new signal – $F_{\text{act}}(\sum S_n)$. This procedure is repeated for all hidden layers.

On the output layer, the signals are summed for the last time, and the outgoing value is activated and denormalized (if necessary). This represents the forecasted value. The forecast is compared with the true value (the training error is calculated), and if the error is above the specified training accuracy, the synaptic weight coefficients are adjusted, and the entire procedure is repeated. Otherwise, the training is considered complete, and the matrix of weight coefficients is saved and can be used for forecasting.

Thus, in neural network-based forecasting of surface displacements caused by mining operations, their function is represented in the additive form of a set of polynomials $\widehat{K}_n$, summed in the neuron of the output layer:

$$K = \sum_{i=1}^{n} \widehat{K}_n = \begin{cases} \widehat{K}_1 = \beta_{11} f_1 + \cdots + \beta_{gl} f_g + \beta_{12} f_1 f_2 + \cdots + \beta_{gl} f_1 f_g + \cdots \\ \cdots \\ \widehat{K}_n = \beta_{n1} f_1 + \cdots + \beta_{nl} f_g + \beta_{n2} f_1 f_2 + \cdots + \beta_{nl} f_1 f_g + \cdots \end{cases}, \quad (1)$$

where β – coefficients of the polynomial functions; f – set of geological factors; n – all possible combinations of polynomial functions $\widehat{K}$ formed by the internal relationships of the artificial neural network; g – quantity of geological factors taken into account; l – number of the neural network layer.

The ellipsis at the end of expression (1) indicates the continuation of the polynomial function, limited only by the dimensionality of the neural network. This type of model is essentially a regression model and serves for the interpolation and extrapolation of values of surface displacement parameters. Thus, it is possible to formulate a computational model that more accurately corresponds to the real object – the geodynamic polygon. Finding a natural dependency of kinematic parameters in the form of a simple analytical relationship is difficult. On the other hand, the computational neural network model is multifactorial (contains a large number of regressors). This is can be formulated as a system of multiple (linear/non-linear) polynomials, the dimensionality of which is constrained by the structure of the artificial neural network model [*Kolmogorov*, 1957].

Currently, there are numerous methods for predicting surface displacement, including deterministic methods, spline functions, polynomial functions, multiple regression, the Shen method, the overlaid triangulation method, kriging, the inverse distance method, and artificial neural networks. However, deterministic methods effectively address only a narrow range of tasks related to modeling movements resulting from a specific process or phenomenon (coseismic deformations, subsidence of the Earth's surface, etc.). Some methods, due to their application, are challenging to interpret as they form intersecting geometric constructions (the inverse distance method, the overlaid triangulation method, the Shen method), while deformation is strictly related to a specific geometrically defined process. Classical methods of geographical interpolation that depend on reference points (kriging, the inverse distance method) do not allow for data extrapolation. Methods of machine learning, particularly artificial neural networks, show a good perspective in this regard [*Boubou et al.*, 2010; *Grishchenkova*, 2017; *Manevich et al.*, 2021; *Manevich and Tatarinov*, 2017; *Tatarinov et al.*, 2018], and their application will be further discussed.

2.2. GNSS data

To test the proposed approach, two regions with different geological conditions and initial data were selected. We use data from several scientific groups that conducted GNSS measurements in the Caucasus region. The initial data for the Caucasus region were derived from GNSS measurements in the Ossetian sector of the Greater Caucasus, as presented in the publication by [*Mironov et al.*, 2021]. These measurements were obtained during field campaigns conducted from 2008 to 2020, as documented in [*Milyukov et al.*, 2015, 2017]. Geodetic points were established to monitor recent crustal movement of the Earth's crust in this region, crossing the Greater Caucasus Range through the territories of the Ossetia. The measurement network was designed to cover this area, and GNSS measurements were conducted at designated geodetic points. The data collection and processing methodology is detailed in [*Milyukov et al.*, 2017; *Mironov et al.*, 2021]. We used the consolidated measurement results presented in the study by [*Mironov et al.*, 2021], which includes displacement data from 60 GNSS points.

2.3. Modeling the horizontal velocity field of the Earth's crust based on discrete irregular geodetic data

2.3.1. ANN structure

The calculations used Python 3, and the results were visualized with the QGIS 3 environment [*Manevich et al.*, 2023]. The Scikit-learn library [*Pedregosa et al.*, 2011] was employed for neural network modeling, which is widely used for such computations. The artificial neural network (ANN) model was specified as a multilayer perceptron using the mlp.regressor function. The following parameters were used for the ANN model: optimizer – adam; activation function – hyperbolic tangent (as it is required for the output data to have both positive and negative values); learning rate – empirically determined and varied from 0.00005 to 0.0001; number of training iterations – from 100,000 to 1,000,000. The architecture of the ANN was as follows:

- quantity of input neurons – equal to the number of features in the model (in this case, six);
- quantity of hidden layers – options with 1 to 3 hidden layers, with 5, 10, and 15 neurons in each layer, were studied;
- quantity of output neurons – 1, for predicting each component of movement separately.

Relatively simple ANN models were employed, which is atypical for machine learning algorithms. This is due to the volume of the data used. Local geodynamic polygons rarely have more than 100 measurement points for such a small amount of data. Constructing complex models leads to a decrease in learning quality and improper tuning of algorithm hyperparameters. In this case, a three-layer perceptron is more than sufficient to address tasks with such a low volume of data. The ANN algorithm was compared with classical interpolation methods – the inverse distance weighting method (with a power parameter $p = 4$), cubic spline, and B-splines (methods implemented in SAGA GIS).

2.3.2. Feature engineering

The input data for the neural network included features characterizing the contrast and intensity of tectonic movements in the research area [*Agayan et al.*, 2020, 2022; *Faber and Domej*, 2021; *Gvishiani et al.*, 2016, 2020], as well as the geographical coordinates of the training and prediction points. These features primarily consisted of geomorphological characteristics associated with morphometric analysis of the terrain. Geological and geophysical data were not applied in this model. Despite their potential, they introduce a number of uncertainties. Spatial data created manually by humans (such as geological maps or tectonic faults) are not formalized data. Therefore, during the algorithm's training process, it adapts to models created by the author based on the original data, rather than creating new relationships between the data. Geophysical fields, such as results from seismic tomography, magnetic and gravitational anomalies, have proven efficiency in applying machine learning methods in Earth sciences as a whole [*Agayan et al.*, 2022; *Aleshin et al.*, 2022; *Dzeboev et al.*, 2019; *Gvishiani et al.*, 2022, 2023; *Sun et al.*, 2022]. In the considered task, they can reflect the deep structure of the Earth's crust and serve as informative features during algorithm training. However, these data are not always available for the areas of interest where research is conducted. Global models of geophysical fields do not always have sufficient detail for their application. In geodynamic polygons with an area of up to 2500 km^2, one cell of the geophysical field dataset can be larger in area than a triangular finite element. Meanwhile, relief data is available with detail down to 30 meters or less (SRTM, ALOS JAXA, ETOPO datasets, and others).

Features were defined within cells. For a geodetic point, the data of which constitute the training set, a hexagonal cell with a radius of the circumscribed circle R is constructed (Figure 2a). The resulting cells are overlaid on the parameter field (feature) for which the value needs to be obtained. Using zonal statistics, the necessary feature is computed in each cell from those mentioned above (average elevation in the cell, range of minimum and maximum elevations, etc.). When forecasting data on a regular grid, the procedure is constructed similarly. The regular grid of cells for which the forecast will be performed is divided (Figure 2b). The necessary features are computed for each cell, which are then

input into the neural network. The forecast result, the displacement components, will be assigned to the centroid of each of the original cells. The following data were used as features:

- coordinates of the cell centroid, in meters, in the universal transverse Mercator projection;
- mean elevation of the terrain in the cell;
- range of elevations in the cell (difference between maximum and minimum values);
- mean density of lineaments in the cell;
- range of lineament density in the cell (difference between maximum and minimum values).

We used the ETOPO1 model as input data [*Amante and Eakins*, 2009]. Lineaments were calculated using the method proposed in [*Sedrette and Rebai*, 2016]. The measure of the dynamic activity index of faults density was determined by using the linear density, which is obtained in a circular vicinity within each cell of the grid. The length of the segment of each line crossed by the circular neighborhood is multiplied by the line weight factor. Then all the length values are summed up and divided by the area of the circle. This process is repeated for all cells in the grid.

The models presented here use a simple feature space. Our goal was to create a simple model, with accessible input data, that can be applied by the widest range of researchers. In addition, simple models are more interpretable than models with complex architecture. The detailed analysis and design of features, their comparison and performance evaluation is an independent study, such as in [*Agayan et al.*, 2022].

2.3.3. Prediction grid and data preprocessing

Equally important is the stage of data preparation and normalization before feeding them into the neural network's input layer. Proper preprocessing of data enables the algorithm to enhance its efficiency and extract valuable information from the data.

A key feature of data preparation is that the displacements need to be transformed into the "no-net-translation" format [*Kaftan and Tatarinov*, 2021] i.e., into the internal displacements of the network. If displacements are provided in the global reference system (as in the work by [*Mironov et al.*, 2021] (Figure 1), it is necessary to subtract from them the mean arithmetic value or the velocity of tectonic plate movement to obtain internal displacements of the geodetic network. This is the format in which the ANN best models the variability of the RCM.

The procedure of declustering data in the context of motion field modeling is discussed. In the preparation of raw data, a situation of overlapping cells can often arise. In this case, the feature values in the cells may be close, while the displacement values can differ significantly. It is necessary to be more attentive to the preparation of raw data and the results of GNSS measurements themselves. Exclude questionable points or points that may be influenced by active exogenous processes or points with poor satellite measurement conditions. In other cases, opposite movements may be caused by local tectonic processes in the research area (such as fault coast displacements) and are important information that should not be removed from the training set. Therefore, in our approach, it is not recommended to apply data declustering, and in cases where two points are in the same location and have different motion indicators, preference is given to the point with the most stable position and a high-quality type of geodetic center. If this parameter is indeterminate, then the point with the longest measurement period is preferred.

The size of the finite element is determined empirically, in accordance with the physical representation of the studied section of the Earth's crust. The Earth's physical crust is not a continuum, so it is not possible to divide the cell into infinitely small elements. When it comes to crustal deformations, the sizes of the sections should be such that changes

in their shape and volume can be interpreted. Normalization of feature data is performed according to standard relationships:

$$\overline{x_j} = \frac{x_j - x_{j0}}{\lambda_j}, \tag{2}$$

where $\overline{x_j}$ – transformed (normalized) value; x_j – the value of the original feature; x_{j0} – the center of variation for the numerical series of the n feature; λ_j – range for the numerical series of the n feature; j – number of values in the numerical series of the n feature.

Different statistics of the original data (minimum, maximum, difference modulus, arithmetic mean, median, zero value, etc.) can be taken as the range and center of variation, depending on empirically determined efficiency. In our study, the arithmetic mean values of the original data sample were taken as the range and center of variation. As a result of data normalization, all features are brought into a consistent system of dimensions, making them numerically comparable and enhancing the efficiency of the neural network's recognition.

The limit prediction radius was determined by the distance at which the feature values in the cells did not change within the range of the original cells. That is, provided that the features in the training sample are distributed the same as in the modeled set.

3. Results

3.1. Methodology for assessing the effectiveness of modeling

For a comprehensive assessment of the effectiveness of modeling methods, it is necessary to plan a series of computational experiments aimed at evaluating the accuracy of forecasting methods in interpolation and extrapolation tasks. One of the best methodologies for assessing performance in data science is cross-validation [*Sun et al.*, 2022]. Cross-validation is a method for evaluating a model to determine how successfully the applied statistical analysis in the model can perform on an independent dataset. Cross-validation methods are successfully applied to assess modeling effectiveness in various Earth sciences [*Agayan et al.*, 2022; *Aleshin et al.*, 2022; *Sun et al.*, 2022], including forecasting recent crustal movement fields [*Bogusz et al.*, 2013].

In this case, the cross-validation method will be applied as follows. The test data set will consist of one point in each iteration of the calculation. All other data will be included in the training data set. In other words, in each iteration of the calculation, surface movements for one point will be calculated based on all other data in the training set. When assessing the quality of the forecast, we average the obtained quality metrics for all test sets.

Earth surface movement data have several characteristic features – they can be multidirectional (have positive or negative signs) and each displacement vector has its own azimuth characterizing the direction of movement. There are a number of errors in forecasts that need to be considered at a detailed and even point level. For example, it is an estimation not only of the absolute magnitude of the predicted displacement/velocity of the RCM, but also of its sign, i.e. its direction. It may happen that one method shows the smallest absolute bias, but recognizes fewer directions of RCM velocities. In this case, the second quality metric will be more correct. Since the directions of movements allow to carry out deformation analysis on compression-tension of the area, which is more important. That is why the development of a program of computational experiments is necessary and it will allow a more correct comparison of the proposed methods. Therefore, the metrics for evaluating the quality of the algorithms' predictions were chosen as follows:

Mean absolute error (MAE) shows the mean absolute deviation of the predicted offsets from the true offsets. The use of absolute deviation is due to the fact that displacement values can be both positive and negative. MAE is determined by formula (3):

$$\mathrm{MAE} = \frac{1}{n}\sum_{i=1}^{n}|U_i - a_i|, \tag{3}$$

where n – quantity of points in the used sample (training, test, control); U_i – the value of measured displacement/velocity; a_i – the value of predicted displacement/velocity.

In addition to quantification, it is necessary to recognize the direction of the motion vector (negative or positive). To evaluate the quality of this aspect, accuracy metrics are defined by formula (4). This evaluation is based on the error matrices of the recognized displacement/velocity classes (Table 1). The accuracy metric allows for estimating the vector of the geodetic point movement direction in the 90° sector. If both components are

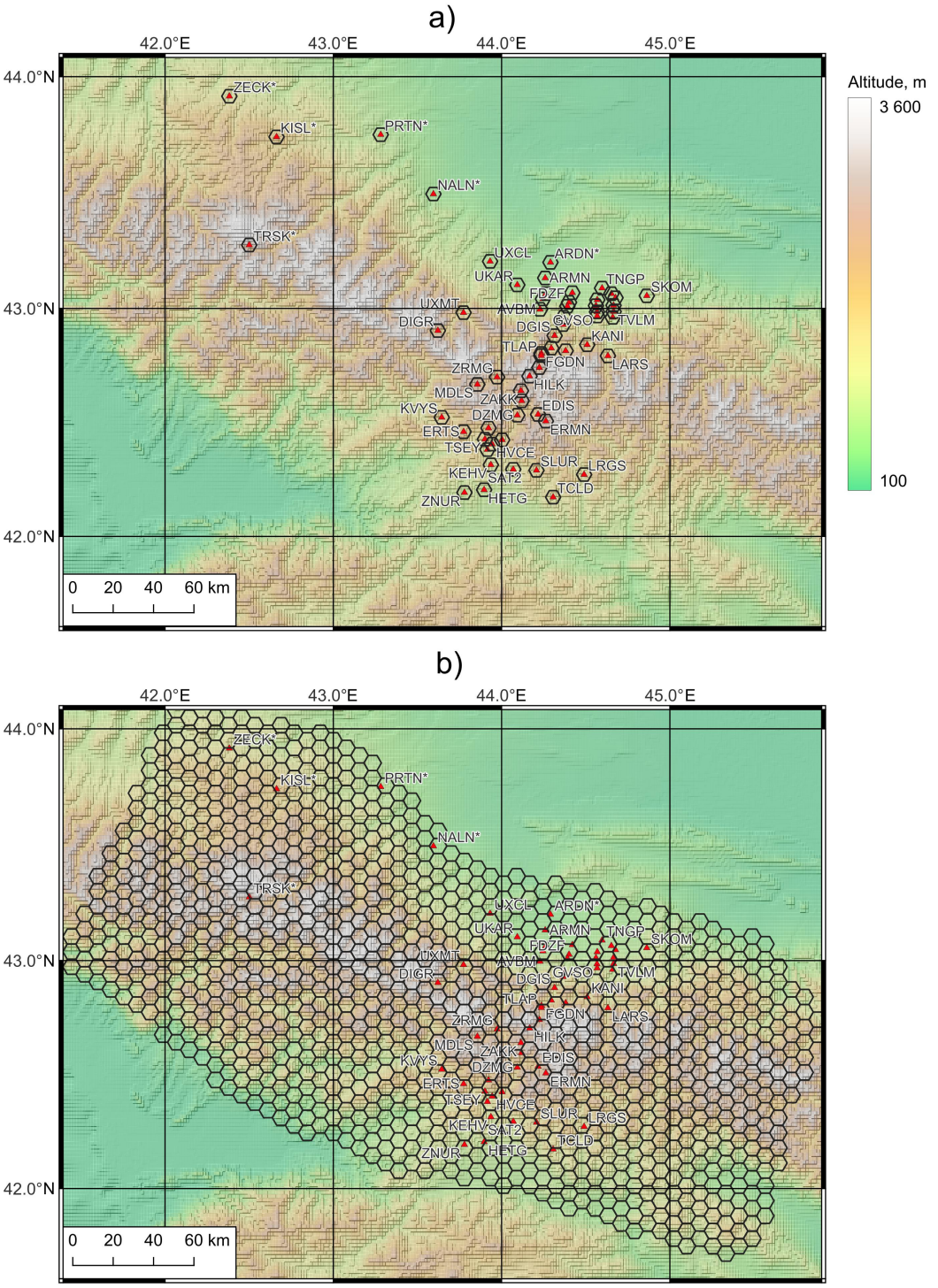

Figure 2. An example of dividing the geodynamic polygon of the Ossetia into cells with $R = 10$ km. a – training set; b – interpolation model with regular cells.

recognized correctly, the modeled value falls into the same direction sector as the true displacement value:

$$\text{accuracy} = \frac{\text{TP+FN}}{\text{TP+FP+FN+TN}}, \tag{4}$$

Table 1. Error matrix (a – the true mark motion vector displacement/velocity, $\hat{a}$ – predicted mark motion vector displacement/velocity)

	$a = 1$	$a = 0$
$\hat{a} = 1$	True Positive (TP)	False Positive (FP)
$\hat{a} = 0$	False Negative (FN)	True Negative (TN)

To evaluate the efficiency of the algorithms, the original data samples are grouped and labeled. All GNSS points are classified into points inside the geodetic network contour (interpolation task) and points outside the geodetic network contour (extrapolation task) (Figure 3). Quality metrics are calculated and compared separately for the groups shown. The points in the control data sample are also classified and analyzed separately from the data used in the modeling.

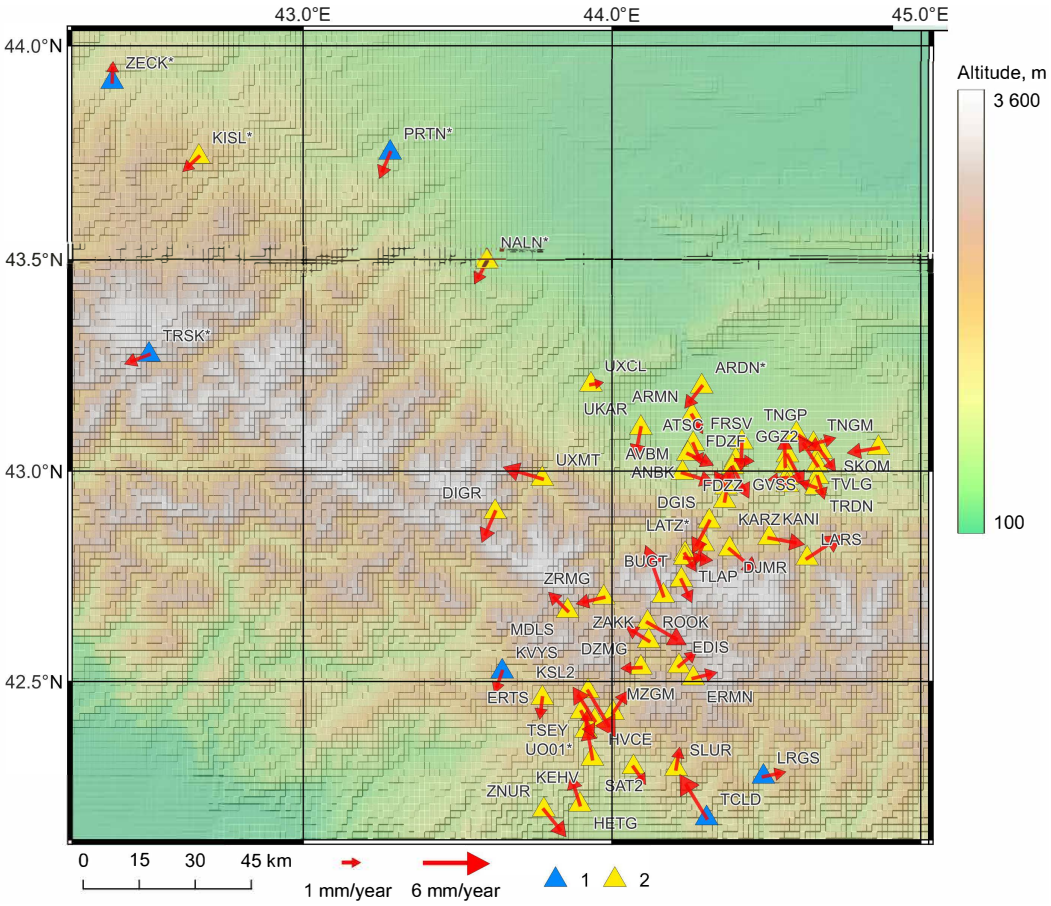

Figure 3. Vectors of geodetic point movements in the internal reference frame and illustration of GNSS point positions outside 1) and inside 2) the geodetic network contour of the Ossetian geodynamic polygon.

Thus, for each data set (from one polygon) the following quality metrics will be calculated:

- MAE – mean absolute deviation of predicted components from the true velocities of motions V_e, V_n in the test sample;

- MAE_extr – mean absolute deviation of predicted components from the true velocities of motions V_e, V_n in the test sample outside in geodetic network (extrapolation points);
- ACC – accuracy of recognizing the direction of the predicted components of motion velocities V_e, V_n (the mean accuracy value is taken for the components V_e, V_n);
- ACC_extr – accuracy of recognizing the direction of the predicted components of motion velocities Ve, Vn in the test sample outside in geodetic network (extrapolation points, the mean accuracy value is taken for the components V_e, V_n);
- ACP – accuracy of recognizing the direction of the predicted velocity vector **V** (the accuracy value is taken for the components V_e, V_n recognized correctly at the same time);
- ACP_extr – accuracy of recognizing the direction of the predicted velocity vector **V** in the test sample outside in the geodetic network (extrapolation points, the accuracy value is taken for the components V_e, V_n recognized correctly at the same time).

These 6 metrics are calculated for each of the algorithms and a comparative evaluation of the modeling performance is performed based on them.

3.2. Results of the Application of ANN for Modeling the RCM field

As a result of the modeling, the components of the RCM were obtained on a regular grid with a step of 10 km (Figure 4). As a result of the modeling, the quality metrics of the cross-validation study on the full dataset and on the extrapolation, dataset were calculated (Table 2).

We analyze the table of the obtained quality metrics of the recent motion field modeling algorithms. The MAE, ACC, ACP rows show the results of calculations of quality metrics for a complete enumeration of the data set. Thus, such a set included points are assigned to the interpolation task and the extrapolation task together. The metrics obtained in this iteration of calculations are very important because they allow to compare the algorithm of artificial neural networks with other algorithms within the framework of the classical problem of interpolation of Earth surface movements. The MAE_extr, ACC_extr, ACP_extr lines contain the results of data extrapolation beyond the geodetic network contour. At the same time, due to the fact that the data are located quite grouped, the estimation for extrapolation points is obtained by classical algorithms. Let us consider in detail the results of quality metrics calculations.

It should also be noted that the level of the mean absolute deviation of the modeled values (both by the ANN algorithm and by classical algorithms) is at or below the RMS of GNSS station velocity definitions (1–3 mm). This result indirectly demonstrates the reliability of the modeled values in the cross-validation sample, as the absolute error of their determination is comparable to the RMS of their definitions.

The following results were obtained for the Ossetian geodynamic polygon. For the full data sample, the metric MAE is between 1.22–2.2 mm. The largest absolute error is obtained when using ANN5,6 architectures and the smallest when using ANN1,9,10 architectures. The classical methods show a range of MAE metric of 1.37–1.65 mm, which on average corresponds to the ANN algorithms. The situation is similar to the mean absolute error on the extrapolation sample (MAE_extr metric). The situation is different with the metric of mean absolute deviations on the extrapolation sample MAE_extr, it lies in the range of 1.04–3.6 mm. The largest absolute error is obtained when using ANN5,6 ANN architecture, and the smallest when using algorithms of inverse distance methods, B-spline, and ANN3,10 architectures. The single-layer and three-layer ANN architectures show lower error on average. The classical algorithms yield a metric range of 1.04–1.63 mm, broadly similar to the full data sample. In terms of mean absolute deviation metrics, ANN1,3,10 architectures show the best results.

For the full data sample, the ACC metric is between 35–56%. The lowest recognition accuracy is obtained using ANN6,11 and the highest recognition accuracy is obtained using ANN3,12 architectures. The classical methods show a range of ACC metric of 43–54%, which is on average higher than the ANN algorithms whose range is 35–56%.

The situation is repeated on the extrapolation dataset. The overall recognition accuracy of ACC_extr lies in the range of 25–66%. The lowest recognition accuracy is obtained using ANN architecture ANN1,6,8,11 and the highest recognition accuracy is obtained using architectures ANN3,4,12, inverse distance method IDP and B-spline. Generally, the ANN architectures show about 40% accuracy in recognizing the direction of the motion components V_e, V_n.

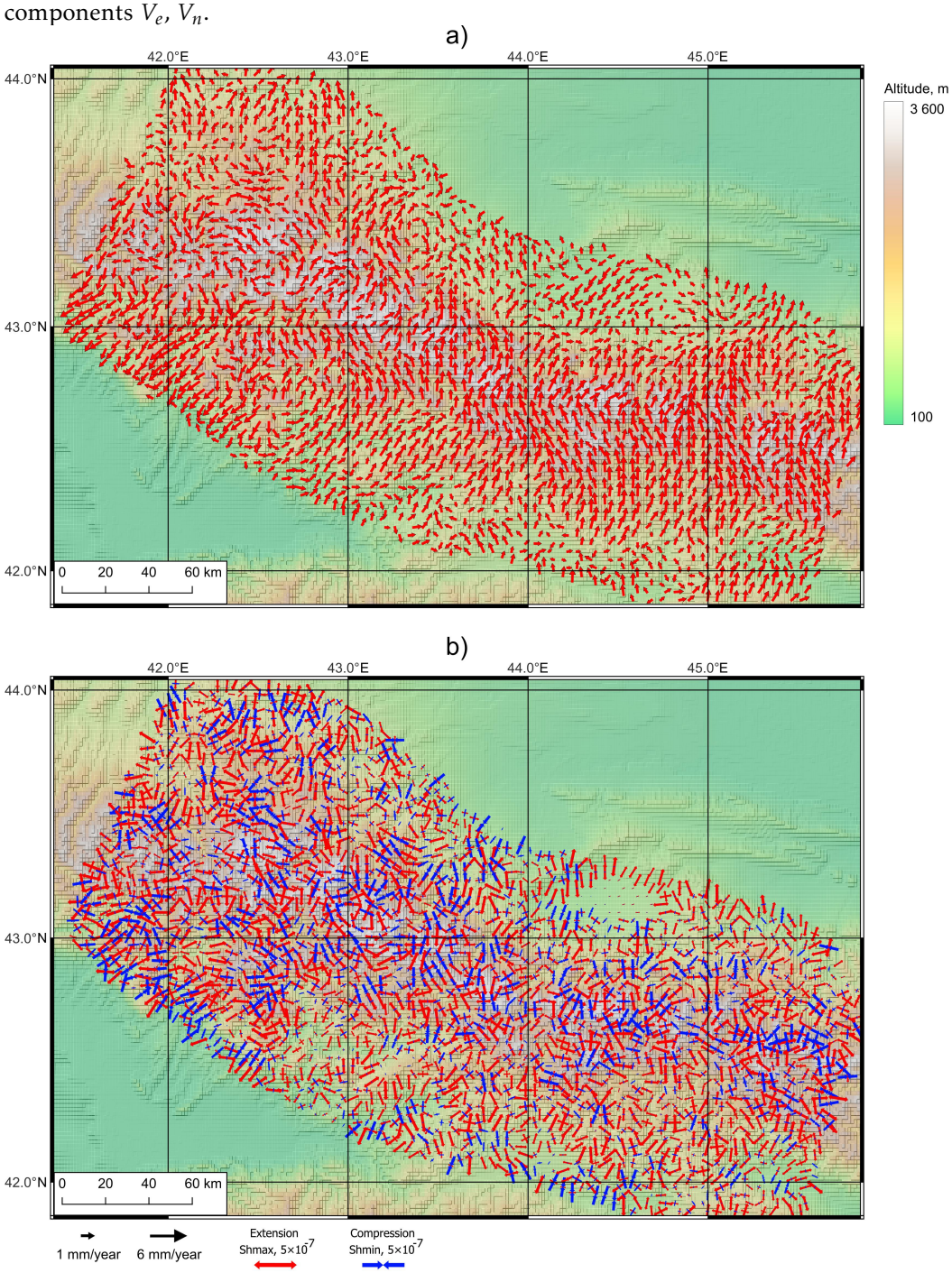

Figure 4. Neural network model of recent crustal movements and deformations of the Ossetian geodynamic polygon: a – field of velocities vectors; b – velocities and orientation axes of main deformations.

For the full data sample, the ACP metric ranges from 8–37%, while the ACP_extr metric ranges from 0–33%. Otherwise, the ACP and ACP_extr metrics show similar results, with the difference that the recognition accuracy is defined in the 90° sector. The lowest

recognition accuracy is obtained using the CBSP algorithm and ANN5,6 architectures, while the highest recognition accuracy is obtained using the IDP inverse distance method and ANN3,12 architectures. The classical methods show an ACP metric range of 12–29%, which is on average lower than that of the ANN algorithms, whose range is 12–37%. The situation is similar to the extrapolation dataset. The lowest recognition accuracy is obtained using the CBSP algorithm and ANN1,2,5,6,7,10,11 architectures, while the highest recognition accuracy is obtained using ANN3,4,12 architectures, IDP and B-spline inverse distance methods.

Among the considered ANN architectures, it is worth highlighting the ANN12 algorithm, which shows the highest and most stable recognition accuracy in terms of ACC and ACP metrics, at the same time having one of the lowest MAE values. If we take a closer look at the results of the cross-validation analysis of ANN1–3 architectures (where single-layer ANNs are also considered), we can see that this result is consistent. It is useful to take it into account when planning the ANN architecture in modeling tasks, where the accuracy of recognition of the direction of the motion vector, rather than approximation to its numerical value, is a higher priority. The most stable of the listed architectures seems to be the ANN8 and ANN11 algorithm. It should be emphasized that a detailed selection of hyperparameters and ANN architecture can improve the above quality metrics. Moreover, the given tables do not give grounds for conclusions about which of the methods or algorithms is unambiguously worse or better. However, in this context, they show the most important thing – the proposed neural network approach confidently shows results not worse than classical methods. Having at the same time the possibility of modeling a wider area. Thus, we can make sure of its adequacy for the use of recent crustal movement field modeling tasks outside the contour of geodetic networks.

Figure 4 illustrates the results of modeling the recent crustal movement field by the algorithm with ANN11 architecture. The figures clearly show that the ANN algorithm makes it possible to obtain the necessary amount of data on a regular grid outside the contour of the geodetic network. Neural network extrapolation allows to obtain data with greater detail of the studied area, where there is a large number of local and large regional tectonic structures. Thus, the analysis of cross-validation results gives encouraging results. We can say that the ANN algorithms within the geodetic network contour model of the RCM field are no worse than classical methods. This conclusion allows us to cautiously conclude that the ANN algorithm in the conditions of limited radius of the modeling area shows itself reasonable and its application is possible for modeling the motion fields outside the contour of the geodetic network. Within the framework of this paper, we did not set ourselves the task of geodynamic interpretation of the obtained motion fields. However, it should be noted that the results of modeling for the Ossetian polygon can be used for geodynamic zoning. At the same time, we can identify zones of tension and compression and calculate the tectonic component of stresses, as well as zones of high-gradient displacements, etc.

4. Discussion

Neural network extrapolation allows us to obtain data with more detail of the studied area, where there are many local and regional tectonic structures. We note the high prospect of using this approach for disparate GNSS data obtained in different epochs of observations. GNSS measurements in the Caucasus, which were started in the 1990s [*Reilinger et al.*, 1997; *Shevchenko et al.*, 1999], are of high interest. Now, they have almost a thirty-year history [*Ismail-Zadeh et al.*, 2020; *Karapetyan et al.*, 2020; *Mironov et al.*, 2021; *Reilinger et al.*, 2006; *Sokhadze et al.*, 2018; *Tibaldi et al.*, 2021]. Measurements of recent crustal movements in the Caucasus are very heterogeneous, as a large number of scientific groups have worked in these regions [*Tibaldi et al.*, 2021]. This makes it difficult to spatially compare the results of their measurements, as they cover different, not completely overlapping areas. The application of machine learning methods will make it possible to model these data onto a single regular grid and obtain digital models of displacements and deformations of the Caucasus territory on a unified scale.

Table 2. Quality metrics of the cross-validation study for data from the Ossetian geodynamic polygon (gradient coloring from red to green corresponds to the reduction of the algorithm's prediction error)

Quality metrics	ANN1	ANN2	ANN3	ANN4	ANN5	ANN6	ANN7	ANN8	ANN9	ANN10	ANN11	ANN12	IDP	MSP	CBSP
MAE, mm	1.22	1.47	1.32	1.51	2.20	2.11	1.40	1.44	1.35	1.28	1.40	1.63	1.43	1.37	1.65
MAE_extr, mm	1.43	1.86	1.25	1.72	2.28	3.60	1.53	1.82	1.94	1.17	1.53	2.37	1.26	1.04	1.63
ACC, %	41.7	45.8	56.3	43.8	37.5	35.4	43.8	35.4	45.8	43.8	35.4	56.3	54.2	43.8	47.9
ACC_extr, %	25.0	41.7	66.7	58.3	41.7	25.0	41.7	25.0	41.7	33.3	25.0	50.0	58.3	50.0	33.3
ACP, %	16.7	20.8	37.5	16.7	8.3	12.5	16.7	12.5	20.8	16.7	16.7	33.3	29.2	20.8	12.5
ACP_extr, %	0.0	0.0	33.3	33.3	0.0	0.0	16.7	0.0	16.7	0.0	0.0	33.3	33.3	33.3	0.0

Gradient coloring

Minimal error — Maximum error

Decoding of abbreviations: Decoding of abbreviations: ANN1 – ANN algorithm, 1 hidden layer, 5 neurons in the hidden layer; ANN2 – ANN algorithm, 1 hidden layer, 10 neurons in the hidden layer; ANN3 – ANN algorithm, 1 hidden layer, 15 neurons in the hidden layer; ANN4 – ANN algorithm, 2 hidden layers, 5 neurons in the hidden layer; ANN5 – ANN algorithm, 2 hidden layers, 10 neurons in the hidden layer; ANN6 – ANN algorithm, 2 hidden layers, 15 neurons in each hidden layer; ANN7 – ANN algorithm, 3 hidden layers, 5 neurons each in the hidden layer; ANN8 – ANN algorithm, 3 hidden layers, 10 neurons each in the hidden layer; ANN9 – ANN algorithm, 3 hidden layers, 15 neurons in each hidden layer; ANN10 – ANN algorithm, 4 hidden layers, 10 neurons per hidden layer; ANN11 – ANN algorithm, 5 hidden layers, 10 neurons each in the hidden layer; ANN12 – ANN algorithm, 1 hidden layer, 50 neurons in the hidden layer; IDP – inverse weighted distance method, degree coefficient $p = 4$; MSP – B-spline; CBSP – cubic spline.

Above we demonstrated a simple application of the algorithm, but, as it was shown in [*Agayan et al.*, 2022], the synthesis of complex geomorphological and geophysical features has great prospects for modeling geodynamic processes, especially on a regional scale. Let us form a feature correlation matrix for the territory of the Greater and Lesser Caucasus, which can also take into account geomorphological and geophysical data. For the scale of studying the whole territory of the Caucasus, a cell size of 50 km was chosen, which allows us to apply large-scale geophysical data (Figure 5).

As is known, the areas of the newest tectonic uplifts in relief often coincide with the places of prevailing denudation, the plunging ones – with the areas of accumulation. Undoubtedly, there is a strong dependence between tectonic movements, the volume of uplifted or lowered matter and the intensity of exogenous denudation, which leads to compensation of tectonic processes. At the same time, if complete compensation does not occur, tectonic movements are directly reflected in the field of absolute heights [*Simonov*, 1998]. In addition to using the main functions of this field (e.g., DEM construction), it can be used to obtain such an important morphometric parameter as surface curvature (horizontal and vertical). The areas of recent crustal movements are reflected not so much in the height field, curvature and steepness of slopes, but also in the density and depth of dissection. The TRI (terrain ruggedness index) [*Różycka et al.*, 2017], a measure of vertical ruggedness in a given neighborhood. It can be considered the most suitable for calculating dismemberment parameters and does not change the geomorphological meaning of this term. In addition, dissection parameters are an expression of the interaction between tectonic movements and erosion processes. In addition to the above, there are more than a hundred [*Negi et al.*, 2023] morphometric indices that directly and indirectly reflect tectonic movements. However, many of them are criticized by geomorphologists, who note that the most important criterion for the correct choice of an index and its meaning should be an indication of the existing geometric or physical image of the most different values within this index.

In addition to these geomorphological indicators, we used geophysical data on the crustal structure of the Greater and Lesser Caucasus for the correlation matrix. We used Bouguer gravity anomalies and the Moho boundary dataset from the Structure and density of sedimentary basins in the Southern part of the East European platform study [*Kaban*

et al., 2021]. As a result, the following indicators were analyzed: the X and Y coordinates of the cell centroid in meters, in the universal transverse Mercator projection; the elevation of the relief in the cell; the density of lineaments in the cell [*Sedrette and Rebai*, 2016]; Bouguer anomalies, Moho surface depth, sediment thickness [*Kaban et al.*, 2021]; surface curvature and TRI terrain dissection index [*Różycka et al.*, 2017]. For each of the indices, we calculated the arithmetic mean, minimum, maximum and range of values within a cell. We calculated the correlation matrix and correlation strength thresholds. The matrix presents Pearson's pairwise correlation coefficient:

$$r = \frac{\sum((x_i - \overline{x}) \times (y_i) - \overline{y})}{\sqrt{\sum (x_i - \overline{x})^2 \times}}.$$

The lower threshold of the correlation relationship was determined using Student's criterion (formula (5)), and the correlation strength intervals using formula (6):

$$r_0 = \frac{t}{\sqrt{t^2 + n - 2}}, \tag{5}$$

$$r_{\text{int}} = \frac{1 - r_0}{3}. \tag{6}$$

Thus, for the set of cells used (691 cells in each of the indicators and the confidence interval of 0.95), the intervals of correlation strength were determined: a weak correlation in the interval 0.0746–0.3831, medium correlation in the interval 0.3831–0.6915, strong correlation in the interval 0.6915–1. The correlation strength was presented as a discrete color scale (Figure 6).

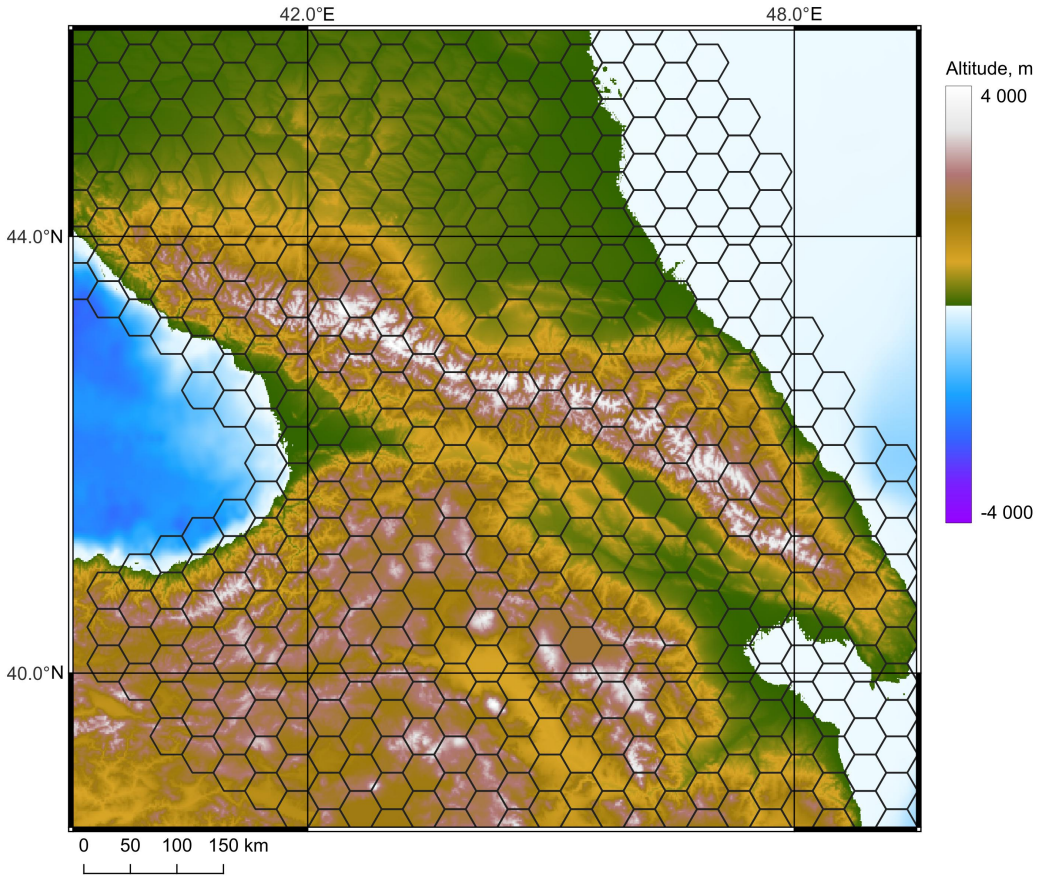

Figure 5. Example of splitting the Caucasus region into cells with R = 50 km.

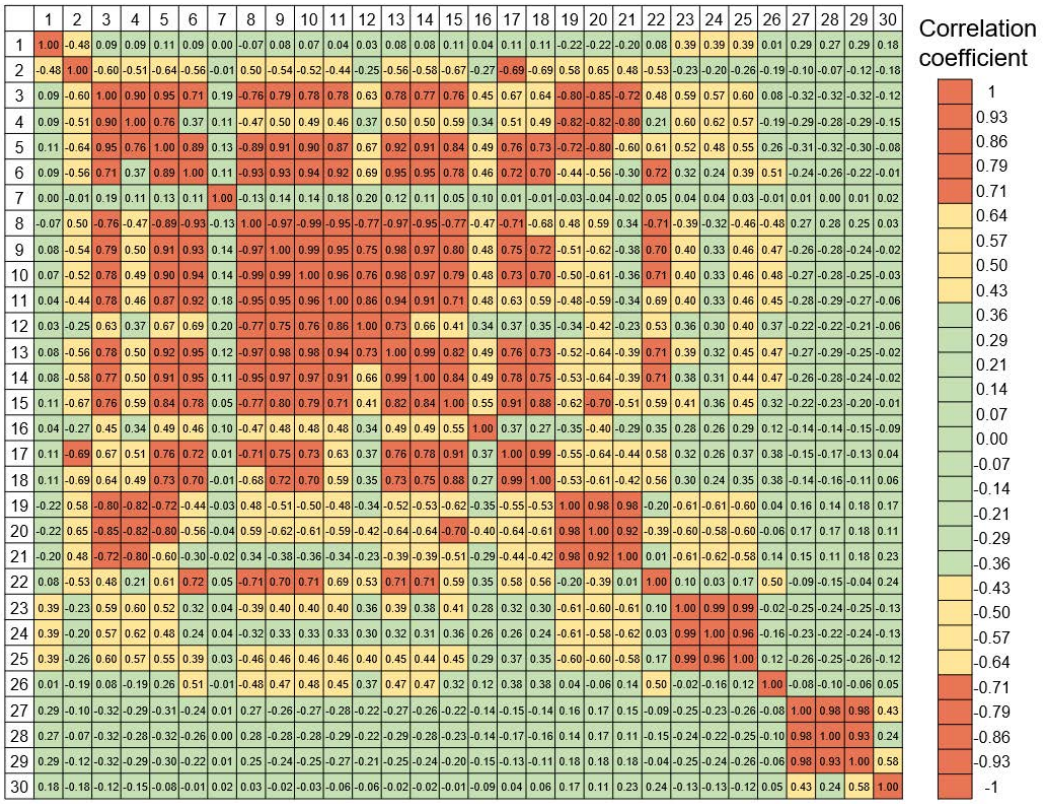

	1	2	3	4	5	6	7	8	9	10	11	12	13	14	15	16	17	18	19	20	21	22	23	24	25	26	27	28	29	30
1	1.00	-0.48	0.09	0.09	0.11	0.09	0.00	-0.07	0.08	0.07	0.04	0.03	0.08	0.08	0.11	0.04	0.11	0.11	-0.22	-0.22	-0.20	0.08	0.39	0.39	0.39	0.01	0.29	0.27	0.29	0.18
2	-0.48	1.00	-0.60	-0.51	-0.64	-0.56	-0.01	0.50	-0.54	-0.52	-0.44	-0.25	-0.56	-0.58	-0.67	-0.27	-0.69	-0.69	0.58	0.65	0.48	-0.53	-0.23	-0.20	-0.26	-0.19	-0.10	-0.07	-0.12	-0.18
3	0.09	-0.60	1.00	0.90	0.95	0.71	0.19	-0.76	0.79	0.78	0.78	0.63	0.78	0.77	0.76	0.45	0.67	0.64	-0.80	-0.85	-0.72	0.48	0.59	0.57	0.60	0.08	-0.32	-0.32	-0.32	-0.12
4	0.09	-0.51	0.90	1.00	0.76	0.37	0.11	-0.47	0.50	0.49	0.46	0.37	0.50	0.50	0.59	0.34	0.51	0.49	-0.82	-0.82	-0.80	0.21	0.60	0.62	0.57	-0.19	-0.29	-0.28	-0.29	-0.15
5	0.11	-0.64	0.95	0.76	1.00	0.89	0.13	-0.89	0.91	0.90	0.87	0.67	0.92	0.91	0.84	0.49	0.76	0.73	-0.72	-0.80	-0.60	0.61	0.52	0.48	0.55	0.26	-0.31	-0.32	-0.30	-0.08
6	0.09	-0.56	0.71	0.37	0.89	1.00	0.11	-0.93	0.93	0.94	0.92	0.69	0.95	0.95	0.78	0.46	0.72	0.70	-0.44	-0.56	-0.30	0.72	0.32	0.24	0.39	0.51	-0.24	-0.26	-0.22	-0.01
7	0.00	-0.01	0.19	0.11	0.13	0.11	1.00	-0.13	0.14	0.14	0.18	0.20	0.12	0.11	0.05	0.10	0.01	-0.01	-0.03	-0.04	-0.02	0.05	0.04	0.04	0.03	-0.01	0.01	0.00	0.01	0.02
8	-0.07	0.50	-0.76	-0.47	-0.89	-0.93	-0.13	1.00	-0.97	-0.99	-0.95	-0.77	-0.97	-0.95	-0.77	-0.47	-0.71	-0.68	0.48	0.59	0.34	-0.71	-0.39	-0.32	-0.46	-0.48	0.27	0.28	0.25	0.03
9	0.08	-0.54	0.79	0.50	0.91	0.93	0.14	-0.97	1.00	0.99	0.95	0.75	0.98	0.97	0.80	0.48	0.75	0.72	-0.51	-0.62	-0.38	0.70	0.40	0.33	0.46	0.47	-0.26	-0.28	-0.24	-0.02
10	0.07	-0.52	0.78	0.49	0.90	0.94	0.14	-0.99	0.99	1.00	0.96	0.76	0.98	0.97	0.79	0.48	0.73	0.70	-0.50	-0.61	-0.36	0.71	0.40	0.33	0.46	0.48	-0.27	-0.28	-0.25	-0.03
11	0.04	-0.44	0.78	0.46	0.87	0.92	0.18	-0.95	0.95	0.96	1.00	0.86	0.94	0.91	0.71	0.48	0.63	0.59	-0.48	-0.59	-0.34	0.69	0.40	0.33	0.46	0.45	-0.28	-0.29	-0.27	-0.06
12	0.03	-0.25	0.63	0.37	0.67	0.69	0.20	-0.77	0.75	0.76	0.86	1.00	0.73	0.66	0.41	0.34	0.37	0.35	-0.34	-0.42	-0.23	0.53	0.36	0.30	0.40	0.37	-0.22	-0.22	-0.21	-0.06
13	0.08	-0.56	0.78	0.50	0.92	0.95	0.12	-0.97	0.98	0.98	0.94	0.73	1.00	0.99	0.82	0.49	0.76	0.73	-0.52	-0.64	-0.39	0.71	0.39	0.32	0.45	0.47	-0.27	-0.29	-0.25	-0.02
14	0.08	-0.58	0.77	0.50	0.91	0.95	0.11	-0.95	0.97	0.97	0.91	0.66	0.99	1.00	0.84	0.49	0.78	0.75	-0.53	-0.64	-0.39	0.71	0.38	0.31	0.44	0.47	-0.26	-0.28	-0.24	-0.02
15	0.11	-0.67	0.76	0.59	0.84	0.78	0.05	-0.77	0.80	0.79	0.71	0.41	0.82	0.84	1.00	0.55	0.91	0.88	-0.62	-0.70	-0.51	0.59	0.41	0.36	0.45	0.32	-0.22	-0.23	-0.20	-0.01
16	0.04	-0.27	0.45	0.34	0.49	0.46	0.10	-0.47	0.48	0.48	0.48	0.34	0.49	0.49	0.55	1.00	0.37	0.27	-0.35	-0.40	-0.29	0.35	0.28	0.26	0.29	0.12	-0.14	-0.14	-0.15	-0.09
17	0.11	-0.69	0.67	0.51	0.76	0.72	0.01	-0.71	0.75	0.73	0.63	0.37	0.76	0.78	0.91	0.37	1.00	0.99	-0.55	-0.64	-0.44	0.58	0.32	0.26	0.37	0.38	-0.15	-0.17	-0.13	0.04
18	0.11	-0.69	0.64	0.49	0.73	0.70	-0.01	-0.68	0.72	0.70	0.59	0.35	0.73	0.75	0.88	0.27	0.99	1.00	-0.53	-0.61	-0.42	0.56	0.30	0.24	0.35	0.38	-0.14	-0.16	-0.11	0.06
19	-0.22	0.58	-0.80	-0.82	-0.72	-0.44	-0.03	0.48	-0.51	-0.50	-0.48	-0.34	-0.52	-0.53	-0.62	-0.35	-0.55	-0.53	1.00	0.98	0.98	-0.20	-0.61	-0.61	-0.60	0.04	0.16	0.14	0.18	0.17
20	-0.22	0.65	-0.85	-0.82	-0.80	-0.56	-0.04	0.59	-0.62	-0.61	-0.59	-0.42	-0.64	-0.64	-0.70	-0.40	-0.64	-0.61	0.98	1.00	0.92	-0.39	-0.60	-0.58	-0.60	-0.06	0.17	0.17	0.18	0.11
21	-0.20	0.48	-0.72	-0.80	-0.60	-0.30	-0.02	0.34	-0.38	-0.36	-0.34	-0.23	-0.39	-0.39	-0.51	-0.29	-0.44	-0.42	0.98	0.92	1.00	0.01	-0.61	-0.62	-0.58	0.14	0.15	0.11	0.18	0.23
22	0.08	-0.53	0.48	0.21	0.61	0.72	0.05	-0.71	0.70	0.71	0.69	0.53	0.71	0.71	0.59	0.35	0.58	0.56	-0.20	-0.39	0.01	1.00	0.10	0.03	0.17	0.50	-0.09	-0.15	-0.04	0.24
23	0.39	-0.23	0.59	0.60	0.52	0.32	0.04	-0.39	0.40	0.40	0.40	0.36	0.39	0.38	0.41	0.28	0.32	0.30	-0.61	-0.60	-0.61	0.10	1.00	0.99	0.99	-0.02	-0.25	-0.24	-0.25	-0.13
24	0.39	-0.20	0.57	0.62	0.48	0.24	0.04	-0.32	0.33	0.33	0.33	0.30	0.32	0.31	0.36	0.26	0.26	0.24	-0.61	-0.58	-0.62	0.03	0.99	1.00	0.96	-0.16	-0.23	-0.22	-0.24	-0.13
25	0.39	-0.26	0.60	0.57	0.55	0.39	0.03	-0.46	0.46	0.46	0.46	0.40	0.45	0.44	0.45	0.29	0.37	0.35	-0.60	-0.60	-0.58	0.17	0.99	0.96	1.00	0.12	-0.26	-0.25	-0.26	-0.12
26	0.01	-0.19	0.08	-0.19	0.26	0.51	-0.01	-0.48	0.47	0.48	0.45	0.37	0.47	0.47	0.32	0.12	0.38	0.38	0.04	-0.06	0.14	0.50	-0.02	-0.16	0.12	1.00	-0.08	-0.10	-0.06	0.05
27	0.29	-0.10	-0.32	-0.29	-0.31	-0.24	0.01	0.27	-0.26	-0.27	-0.28	-0.22	-0.27	-0.26	-0.22	-0.14	-0.15	-0.14	0.16	0.17	0.15	-0.09	-0.25	-0.23	-0.26	-0.08	1.00	0.98	0.98	0.43
28	0.27	-0.07	-0.32	-0.28	-0.32	-0.26	0.00	0.28	-0.28	-0.28	-0.29	-0.22	-0.29	-0.28	-0.23	-0.14	-0.17	-0.16	0.14	0.17	0.11	-0.15	-0.24	-0.22	-0.25	-0.10	0.98	1.00	0.93	0.24
29	0.29	-0.12	-0.32	-0.29	-0.30	-0.22	0.01	0.25	-0.24	-0.25	-0.27	-0.21	-0.25	-0.24	-0.20	-0.15	-0.13	-0.11	0.18	0.18	0.18	-0.04	-0.25	-0.24	-0.26	-0.06	0.98	0.93	1.00	0.58
30	0.18	-0.18	-0.12	-0.15	-0.08	-0.01	0.02	0.03	-0.02	-0.03	-0.06	-0.06	-0.02	-0.02	-0.01	-0.09	0.04	0.06	0.17	0.11	0.23	0.24	-0.13	-0.13	-0.12	0.05	0.43	0.24	0.58	1.00

Figure 6. Correlation matrix of geomorphological and geophysical features of the Caucasus region: 1 – X coordinates; 2 – Y coordinates; 3 – arithmetic mean value of relief in a cell; 4 – minimum value of relief in a cell; 5 – maximum value of relief in a cell; 6 – range of relief values in a cell (max–min); 7 – arithmetic mean value of curvature in a cell; 8 – minimum value of curvature in a cell; 9 – maximum value of curvature in the cell; 10 – range of curvature values in the cell (max–min); 11 – arithmetic mean value of TRI index in the cell; 12 – minimum value of TRI index in the cell; 13 – maximum value of TRI index in the cell; 14 – range of TRI index values in the cell (max–min); 15 – arithmetic mean value of lineament density in the cell; 16 – minimum value of lineament density in the cell; 17 – maximum value of lineament density in the cell; 18 – range of lineament density values in the cell (max–min); 19 – arithmetic mean of Bouguer anomalies in the cell; 20 – minimum value of Bouguer anomalies in the cell; 21 – maximum value of Bouguer anomalies in the cell; 22 – range of Bouguer anomalies in the cell (max–min); 23 – arithmetic mean of Moho surface values in the cell; 24 – minimum value of Moho surface in the cell; 25 – maximum value of Bouguer anomalies in the cell; 26 – range of Moho surface values in the cell (max–min); 27 – arithmetic mean of precipitation power values in the cell; 28 – minimum value of precipitation power in the cell; 29 – maximum value of precipitation power in the cell; 30 – range of precipitation power values in the cell (max–min).

The correlation matrix of geomorphological and geophysical features was analyzed (Figure 6). 200 out of 435 values of correlation of features have weak correlation. This is a good indicator from the point of view of data analysis, because the features must be non-collinear, otherwise, the generalization ability of the neural network algorithm is reduced due to the high variance of the data. Medium and strong correlations are found within the feature groups of relief, curvature, TRI index and lineament density. This is true since all these indices were calculated from the same initial data. The exceptions are certain calculated indices, such as the average value of curvature in a cell (absolutely not correlated with any data), the minimum values of TRI index in a cell and the minimum values of lineament density in a cell. Similarly, medium and strong correlations are formed within groups of the same geophysical indicator features (Bouguer anomalies, Moho boundary and sediment thickness). Other groups of geophysical attributes have on average weak correlation relations. In general, the best results show signs related to sediment thickness –

weak correlation with all other parameters. Mostly weak and average correlations have signs of Moho boundary and Bouguer anomaly. They are more strongly correlated with geomorphological features.

In general, weak correlations between features characterize these indicators as reflecting different properties of the geological environment and are independent datasets for the conditions of the Caucasus region. However, the application of such a dataset is only possible on a small scale with a specified cell size of 50 km. Since the geophysical models used have low spatial resolution and the chosen radius allows to cover the area with some degree of variability. Cells with a smaller radius would perform worse under these conditions.

5. Conclusions

Spatial modeling based on the neural network approach allows to model adequately the fields of recent crustal movements and deformations outside the geodetic network contour. The paper details the settings of hyperparameters and the justification of the applicability of the neural network model for the tasks of forecasting crustal velocity fields. The results presented in comparison with classical modeling methods show that the neural network approach shows results not worse than classical methods. However, the ANN algorithm has an important property – it can extrapolate data beyond the contour of the geodetic network. Comparison of quality metrics of classical methods and neural network approach shows the adequacy of ANN results, which allows us to apply them in the tasks of large-scale modeling of the RCM field. Neural network extrapolation allows us to obtain data with greater detail of the studied area, where there are a lot of local and regional tectonic structures.

The possibility of designing and applying more complex features for the neural network based on geomorphological and geophysical data is considered. As a discussion, we note the prospect of first of all using geomorphological indicators as a feature space for modeling the RCM field. In the presented models, the objective was not to construct a complex feature space. On the contrary, the aim was to create a simple model, with available input data, that can be applied by the widest range of researchers. In addition, simple models are more interpretable than models with complex architecture.

The application of such an approach to disparate GNSS data obtained in different epochs of observations is very promising. Of high interest are the GNSS measurements in the Caucasus, which are very heterogeneous, since a large number of scientific groups worked in these regions. The application of machine learning methods will allow the modeling of these data on a single regular grid and obtaining digital models of displacements and deformations of the Caucasus territory on a unified scale. The use of geomorphological indicators as a feature space for modeling the RCM field is a promising approach. Since it is the relief that reflects tectonic movements, both recent and modern, which is especially pronounced in the tectonically active region of the Caucasus.

Acknowledgments. The research was supported by Russian science foundation "System Seismic Hazard Assessment of the Central Part of the Greater Caucasus (Ossetian sector)" (project #23-17-00176). This work employed facilities and data provided by the Shared Research Facility "Analytical Geomagnetic Data Center" of the Geophysical Center of RAS (http://ckp.gcras.ru/).

References

Agayan, S. M., V. N. Tatarinov, A. D. Gvishiani, S. R. Bogoutdinov, and I. O. Belov (2020), FDPS algorithm in stability assessment of the Earth's crust structural tectonic blocks, *Russian Journal of Earth Sciences*, *20*, ES6014, https://doi.org/10.2205/2020ES000752.

Agayan, S. M., I. V. Losev, I. O. Belov, V. N. Tatarinov, A. I. Manevich, and M. A. Pasishnichenko (2022), Dynamic Activity Index for Feature Engineering of Geodynamic Data for Safe Underground Isolation of High-Level Radioactive Waste, *Applied Sciences*, *12*(4), 2010, https://doi.org/10.3390/app12042010.

Aki, K. (1968), Seismic displacements near a fault, *Journal of Geophysical Research*, *73*(16), 5359–5376, https://doi.org/10.1029/JB073i016p05359.

Aleshin, I., K. Kholodkov, I. Malygin, R. Shevchuk, and R. Sidorov (2022), Geomagnetic Survey Interpolation with the Machine Learning Approach, *Russian Journal of Earth Sciences*, *22*, https://doi.org/10.2205/2022ES000818.

Allmendinger, R. W., N. Cardozo, and D. M. Fisher (2011), *Structural Geology Algorithms: Vectors and Tensors*, Cambridge University Press, https://doi.org/10.1017/CBO9780511920202.

Amante, C., and B. W. Eakins (2009), ETOPO1 1 Arc-Minute Global Relief Model: Procedures, Data Sources and Analysis.

Anantrasirichai, N., J. Biggs, F. Albino, P. Hill, and D. Bull (2018), Application of Machine Learning to Classification of Volcanic Deformation in Routinely Generated InSAR Data, *Journal of Geophysical Research: Solid Earth*, *123*(8), 6592–6606, https://doi.org/10.1029/2018jb015911.

Batugin, A., V. Ogadzhanov, S. Han, S. Shevchuk, S. Kostikov, and A. Oborin (2022), Exploring the Nature of Seismic Events in the Underground Gas Storages Area of the Volga Federal District, *Russian Journal of Earth Sciences*, *22*, https://doi.org/10.2205/2022ES000819.

Bogusz, J., A. Kłos, P. Grzempowski, and B. Kontny (2013), Modelling the Velocity Field in a Regular Grid in the Area of Poland on the Basis of the Velocities of European Permanent Stations, *Pure and Applied Geophysics*, *171*(6), 809–833, https://doi.org/10.1007/s00024-013-0645-2.

Boubou, R., F. Emeriault, and R. Kastner (2010), Artificial neural network application for the prediction of ground surface movements induced by shield tunnelling, *Canadian Geotechnical Journal*, *47*(11), 1214–1233, https://doi.org/10.1139/T10-023.

Cardozo, N., and R. W. Allmendinger (2009), SSPX: A program to compute strain from displacement/velocity data, *Computers & Geosciences*, *35*(6), 1343–1357, https://doi.org/10.1016/j.cageo.2008.05.008.

Dimitrios, G. A., X. Papanikolaou, A. Ganas, and D. Paradissis (2019), StrainTool: A software package to estimate strain tensor parameters (Version v1.0).

Dokukin, P. A., V. I. Kaftan, and R. I. Krasnoperov (2010), Influence of triangle shape in geodetic network on the results of definition of Earth surface deformations, *Izvestia vuzov. Geodesy and aerophotosurveying*, *5*, 6–11 (in Russian).

Dzeboev, B. A., A. A. Soloviev, B. V. Dzeranov, J. K. Karapetyan, and N. A. Sergeeva (2019), Strong earthquake-prone areas recognition based on the algorithm with a single pure training class. II. Caucasus, M ≥ 6.0. Variable EPA method, *Russian Journal of Earth Sciences*, *19*(6), https://doi.org/10.2205/2019ES000691.

Esikov, N. P. (1979), *Tectonophysical aspects of analysis of recent Earth's surface movements*, Nauka, Novosibirsk.

Faber, R., and G. Domej (2021), 3D Computer-Assisted Geological Mapping: Testing WinGeol's FaultTrace for semi-automatic structural geological assessment, *Russian Journal of Earth Sciences*, *21*(1), https://doi.org/10.2205/2020ES000757.

Ghiasi, Y., and V. Nafisi (2015), The improvement of strain estimation using universal kriging, *Acta Geodaetica et Geophysica*, *50*(4), 479–490, https://doi.org/10.1007/s40328-015-0103-y.

Goudarzi, M. A., M. Cocard, and R. Santerre (2015), GeoStrain: An open source software for calculating crustal strain rates, *Computers & Geosciences*, *82*, 1–12, https://doi.org/10.1016/j.cageo.2015.05.007.

Grishchenkova, E. N. (2017), Development of a Neural Network for Earth Surface Deformation Prediction, *Geotechnical and Geological Engineering*, *36*(4), 1953–1957, https://doi.org/10.1007/s10706-017-0438-y.

Gvishiani, A. D., B. A. Dzeboev, and S. M. Agayan (2016), FCaZm intelligent recognition system for locating areas prone to strong earthquakes in the Andean and Caucasian mountain belts, *Izvestiya, Physics of the Solid Earth*, *52*(4), 461–491, https://doi.org/10.1134/s1069351316040017.

Gvishiani, A. D., A. A. Soloviev, and B. A. Dzeboev (2020), Problem of Recognition of Strong-Earthquake-Prone Areas: a State-of-the-Art Review, *Izvestiya, Physics of the Solid Earth*, *56*(1), https://doi.org/10.1134/S1069351320010048.

Gvishiani, A. D., M. N. Dobrovolsky, B. V. Dzeranov, and B. A. Dzeboev (2022), Big Data in Geophysics and Other Earth Sciences, *Izvestiya, Physics of the Solid Earth*, *58*(1), https://doi.org/10.1134/S1069351322010037 (in Russian).

Gvishiani, A. D., V. Y. Panchenko, and I. M. Nikitina (2023), System analysis of big data for Earth sciences, *Herald of the Russian Academy of Sciences*, *93*(6), 518–525, https://doi.org/10.31857/S0869587323060087 (in Russian).

IAEA-TECDOC-1987 (2021), An Introduction to Probabilistic Fault Displacement Hazard Analysis in Site Evaluation for Existing Nuclear Installation.

Ismail-Zadeh, A., S. Adamia, A. Chabukiani, T. Chelidze, and other (2020), Geodynamics, seismicity, and seismic hazards of the Caucasus, *Earth-Science Reviews*, *207*, 103,222, https://doi.org/10.1016/j.earscirev.2020.103222.

Kaban, M. K., A. Gvishiani, R. Sidorov, A. Oshchenko, and R. I. Krasnoperov (2021), Structure and Density of Sedimentary Basins in the Southern Part of the East-European Platform and Surrounding Area, *Applied Sciences*, *11*(2), 512, https://doi.org/10.3390/app11020512.

Kaftan, V. I., and V. N. Tatarinov (2021), An Analysis of Possibilities of GNSS Local Strain Monitoring Networks in Earthquake-Prone Areas, *Journal of Volcanology and Seismology*, *15*(6), 379–386, https://doi.org/10.1134/S074204632106004X.

Karapetyan, J. K., R. S. Sargsyan, K. S. Kazaryan, B. V. Dzeranov, B. A. Dzeboev, and R.-K. Karapetyan (2020), Current state of exploration and actual problems of tectonics, seismology and seismotectonics of Armenia, *Russian Journal of Earth Sciences*, *20*(2), https://doi.org/10.2205/2020es000709.

Kolmogorov, A. N. (1957), On the representation of continuous functions of many variables by superposition of continuous functions of one variable and addition, *Doklady Akademii Nauk SSSR*, *114*(5), 953–956 (in Russian).

Kolmogorova, P. P., and G. I. Karataev (1975), Prediction of the velocities of modern vertical movements of the Earth's crust by the correlation model from statistical geological and geophysical data, in *Methodical issues of the study of modern movements of the Earth's crust*, pp. 182–203, IGM SB RAS (in Russian).

Kuzmin, Y. O. (2020), Topical issues of use of geodetic measurements at geodynamic monitoring of objects of oil and gas complex, *Vestnik SSUGT (Siberian State University of Geosystems and Technologies)*, *25*(1), 43–54, https://doi.org/10.33764/2411-1759-2020-25-1-43-54.

Lei, Q., and S. Loew (2021), Modelling coseismic displacements of fracture systems in crystalline rock during large earthquakes: Implications for the safety of nuclear waste repositories, *International Journal of Rock Mechanics and Mining Sciences*, *138*, 104,590, https://doi.org/10.1016/j.ijrmms.2020.104590.

Manevich, A., V. Kaftan, R. Shevchuk, and D. Urmanov (2021), Modelling the horizontal velocity field of the Nizhne-Kansk massif according to GNSS Observations, *ENVIRONMENT. TECHNOLOGIES. RESOURCES. Proceedings of the International Scientific and Practical Conference*, *1*, 162–169, https://doi.org/10.17770/etr2021vol1.6545.

Manevich, A. I., and V. N. Tatarinov (2017), Application of artificial neural networks for forecasting modern crustal movements, in *Geoinformation technologies - a tool for increasing the efficiency and safety of mining*, vol. 5, pp. 37–48, Geophisical Center RAS (in Russian).

Manevich, A. I., R. V. Shevchuk, V. I. Kaftan, V. N. Tatarinov, and S. M. Zabrodin (2022), Improvement of the gnss monitoring network of the nizhne-kansky massif using a bedrock pin geodetic center, *Seismic Instruments*, *58*(S2), S267–S280, https://doi.org/10.3103/s0747923922080084.

Manevich, A. I., R. V. Shevchuk, I. V. Losev, V. I. Kaftan, D. I. Urmanov, and A. I. Shakirov (2023), PyGeoStrain: A software package for calculation crustal strain (v1.0).

Markovich, K. I. (2020), Prediction of velocities of modern vertical movements of the earth's crust from geodetic, geophysical and seismological data, *Geodynamics & Tectonophysics*, *11*(2), 365–377, https://doi.org/10.5800/GT-2020-11-2-0480.

Matheron, G. (1970), Random Functions and their Application in Geology, in *Geostatistics*, pp. 79–87, Springer US, https://doi.org/10.1007/978-1-4615-7103-2_7.

Mazurov, B. T. (2016), Geodynamic system (kinematic and deformation model of block movements), *Vestnik SSUGT*, *3*(35), 5–15 (in Russian).

Milyukov, V. K., A. P. Mironov, G. M. Steblov, V. I. Shevchenko, A. G. Kusraev, V. N. Drobyshev, and K. M. Khubaev (2015), The contemporary GPS-derived horizontal motions of the main elements of tectonic structure in the Ossetian segment of Greater Caucasus, *Izvestiya*, *Physics of the Solid Earth*, *51*(4), 522–534, https://doi.org/10.1134/S1069351315040072.

Milyukov, V. K., A. P. Mironov, G. M. Steblov, A. N. Ovsyuchenko, E. A. Rogozhin, V. N. Drobyshev, A. G. Kusraev, K. M. Khubaev, and K.-M. Z. Torchinov (2017), Satellite geodetic monitoring of the Vladikavkaz active fault zone: First results, *Izvestiya*, *Physics of the Solid Earth*, *53*(4), 598–605, https://doi.org/10.1134/S1069351317040061.

Mironov, A. P., V. K. Milyukov, G. M. Steblov, V. N. Drobyshev, A. G. Kusraev, and K. M. Khubaev (2021), Crustal Strains in the Ossetian Region of the Greater Caucasus Based on GNSS Measurements, *Izvestiya*, *Atmospheric and Oceanic Physics*, *57*(11), 1498–1513, https://doi.org/10.1134/S0001433821110074.

Moss, R. E. S., and Z. E. Ross (2011), Probabilistic Fault Displacement Hazard Analysis for Reverse Faults, *Bulletin of the Seismological Society of America*, *101*(4), 1542–1553, https://doi.org/10.1785/0120100248.

Negi, P., A. Goswami, and G. C. Joshi (2023), Geomorphic indices based topographic characterization of Alaknanda catchment, Western Himalaya using spatial data, *Environmental Earth Sciences*, *82*(20), https://doi.org/10.1007/s12665-023-11158-w.

Nurminen, F., P. Boncio, F. Visini, B. Pace, A. Valentini, S. Baize, and O. Scotti (2020), Probability of Occurrence and Displacement Regression of Distributed Surface Rupturing for Reverse Earthquakes, *Frontiers in Earth Science*, *8*, https://doi.org/10.3389/feart.2020.581605.

Okada, Y. (1992), Internal deformation due to shear and tensile faults in a half-space, *Bulletin of the Seismological Society of America*, *82*(2), 1018–1040, https://doi.org/10.1785/BSSA0820021018.

Pedregosa, F., G. Varoquaux, A. Gramfort, V. Michel, B. Thirion, and other (2011), Scikit-learn: Machine Learning in Python, *Journal of Machine Learning Research*, *12*, 2825–2830.

Petrov, V. A., V. A. Minaev, S. A. Ustinov, I. O. Nafigin, and A. B. Lexin (2021), Assessment of Seismogeodynamic Activity of Mining Areas on the Basis of 3D Geoinformation Modeling, *Russian Journal of Earth Sciences*, *21*(6), https://doi.org/10.2205/2021ES000781.

Reilinger, R., S. McClusky, P. Vernant, S. Lawrence, S. Ergintav, R. Cakmak, and other (2006), GPS constraints on continental deformation in the Africa-Arabia-Eurasia continental collision zone and implications for the dynamics of plate interactions, *Journal of Geophysical Research: Solid Earth*, *111*(B5), https://doi.org/10.1029/2005JB004051.

Reilinger, R. E., S. C. McClusky, B. J. Souter, M. W. Hamburger, M. T. Prilepin, A. Mishin, T. Guseva, and S. Balassanian (1997), Preliminary estimates of plate convergence in the Caucasus Collision Zone from global positioning system measurements, *Geophysical Research Letters*, *24*(14), 1815–1818, https://doi.org/10.1029/97gl01672.

Różycka, M., P. Migoń, and A. Michniewicz (2017), Topographic Wetness Index and Terrain Ruggedness Index in geomorphic characterisation of landslide terrains, on examples from the Sudetes, SW Poland, *Zeitschrift für Geomorphologie*, *Supplementary Issues*, *61*(2), 61–80, https://doi.org/10.1127/zfg_suppl/2016/0328.

Sandwell, D. T. (1987), Biharmonic Spline Interpolation of GEOS-3 and SEASAT Altimeter Data, *Geophysical Research Letters*, *14*(2), 139–142.

Sedrette, S., and N. Rebai (2016), Automatic extraction of lineaments from Landsat Etm+ images and their structural interpretation: Case Study in Nefza region (North West of Tunisia), *Journal of Research in Environmental and Earth Sciences*, *4*, 139–145.

Shen, Z., D. D. Jackson, and B. X. Ge (1996), Crustal deformation across and beyond the Los Angeles basin from geodetic measurements, *Journal of Geophysical Research: Solid Earth*, *101*(B12), 27,957–27,980, https://doi.org/10.1029/96JB02544.

Shen, Z., M. Wang, Y. Zeng, and F. Wang (2015), Optimal Interpolation of Spatially Discretized Geodetic Data, *Bulletin of the Seismological Society of America*, *105*(4), 2117–2127, https://doi.org/10.1785/0120140247.

Shevchenko, V. I., T. V. Guseva, A. A. Lukk, A. V. Mishin, and other (1999), Modern geodynamics of the Caucasus (based on GPS measurements and seismological data), *Izvestiya, Physics of the Solid Earth*, *9*, 3–18 (in Russian).

Simonov, Y. G. (1998), *Morphometric analysis of relief*, SGU Publishing House, Moscow-Smolensk (in Russian).

Sokhadze, G., M. Floyd, T. Godoladze, R. King, E. S. Cowgill, Z. Javakhishvili, G. Hahubia, and R. Reilinger (2018), Active convergence between the Lesser and Greater Caucasus in Georgia: Constraints on the tectonic evolution of the Lesser–Greater Caucasus continental collision, *Earth and Planetary Science Letters*, *481*, 154–161, https://doi.org/10.1016/j.epsl.2017.10.007.

Srivastava, H., and E. Isaaks (1989), *An Introduction to Applied Geostatistics*, Oxford University Press.

Sun, Z., L. Sandoval, R. Crystal-Ornelas, S. M. Mousavi, J. Wang, C. Lin, and other (2022), A review of Earth Artificial Intelligence, *Computers & Geosciences*, *159*, 105,034, https://doi.org/10.1016/j.cageo.2022.105034.

Tatarinov, V. N., A. I. Manevich, and I. V. Losev (2018), A system approach to geodynamic zoning based on artificial neural networks, *Mining science and technology*, (3), 14–25, https://doi.org/10.17073/2500-0632-2018-3-14-25 (in Russian).

Tatarinov, V. N., V. N. Morozov, and A. S. Batugin (2019), An underground research laboratory: new opportunities in the study of the stress-strain state and dynamics of rock mass destruction, *Russian Journal of Earth Sciences*, *19*, ES2002, https://doi.org/10.2205/2019ES000659 (in Russian).

Teza, G., A. Pesci, and A. Galgaro (2008), Grid_strain and grid_strain3: Software packages for strain field computation in 2D and 3D environments, *Computers & Geosciences*, *34*(9), 1142–1153, https://doi.org/10.1016/j.cageo.2007.07.006.

Tibaldi, A., F. L. Bonali, E. Russo, and N. Corti (2021), Active Kinematics of the Greater Caucasus from Seismological and GPS Data: A Review, in *Building Knowledge for Geohazard Assessment and Management in the Caucasus and other Orogenic Regions*, NATO Science for Peace and Security Series C: Environmental Security, pp. 33–57, Springer Netherlands, https://doi.org/10.1007/978-94-024-2046-3.

Wackernagel, H. (1994), *Multivariate Geostatistics*, Springer, Berlin, Germany.

Wu, J., C. Tang, and Y. Chen (2003), Effect of triangle shape factor on precision of crustal deformation calculated, *Journal of Geodesy and Geodynamics*, *23*(3), 26–30.

Yamaga, N., and Y. Mitsui (2019), Machine Learning Approach to Characterize the Postseismic Deformation of the 2011 Tohoku-Oki Earthquake Based on Recurrent Neural Network, *Geophysical Research Letters*, *46*(21), https://doi.org/10.1029/2019gl084578.

Yang, B., K. Yin, S. Lacasse, and Z. Liu (2019), Time series analysis and long short-term memory neural network to predict landslide displacement, *Landslides*, *16*(4), 677–694, https://doi.org/10.1007/s10346-018-01127-x.

Youngs, R. R., W. J. Arabasz, R. E. Anderson, A. R. Ramelli, J. P. Ake, D. B. Slemmons, and other (2003), A Methodology for Probabilistic Fault Displacement Hazard Analysis (PFDHA), *Earthquake Spectra*, *19*(1), 191–219, https://doi.org/10.1193/1.1542891.